

Bias dependence and correlation of the cathodoluminescence and electron beam induced current from an InGaN/GaN light emitting diode

M. J. Wallace,¹ P. R. Edwards,¹ M. J. Kappers,² M. A. Hopkins,³ F. Oehler,² S. Sivaraya,³ D. W. E. Allsopp,³ R. A. Oliver,² C. J. Humphreys,² and R. W. Martin¹

¹Department of Physics, SUPA, University of Strathclyde, Glasgow G4 0NG, United Kingdom

²Department of Materials Science and Metallurgy, University of Cambridge, Cambridge CB2 3QZ, United Kingdom

³Department of Electronic and Electrical Engineering, University of Bath, Bath BA2 7AY, United Kingdom

(Received 7 February 2014; accepted 6 July 2014; published online 18 July 2014)

Micron-scale mapping has been employed to study a contacted InGaN/GaN LED using combined electroluminescence (EL), cathodoluminescence (CL), and electron beam induced current (EBIC). Correlations between parameters, such as the EBIC and CL intensity, were studied as a function of applied bias. The CL and EBIC maps reveal small areas, 2–10 μm in size, which have increased nonradiative recombination rate and/or a lower conductivity. The CL emission from these spots is blue shifted, by 30–40 meV. Increasing the reverse bias causes the size of the spots to decrease, due to competition between in-plane diffusion and drift in the growth direction. EL mapping shows large bright areas ($\sim 100 \mu\text{m}$) which also have increased EBIC, indicating domains of increased conductivity in the p and/or n -GaN. © 2014 Author(s). All article content, except where otherwise noted, is licensed under a Creative Commons Attribution 3.0 Unported License.

[<http://dx.doi.org/10.1063/1.4890497>]

I. INTRODUCTION

Progress in the field of gallium nitride optoelectronics has been rapid over the last decade or so, with blue and white light emitting diodes (LEDs) and laser diodes firmly embedded in the marketplace. With this commercialization, there is a growing interest in the effects of variations in the LED microstructure of device performance.¹ Cathodoluminescence (CL) is a powerful technique for probing the luminescence characteristics of LED structures due to its high spatial resolution and range of excitation conditions. Panchromatic and monochromatic CL mapping provide spatial information on the variation in intensity, of either the total luminescence or that of a single band, respectively. CL *hyperspectral imaging*—the recording of a full spectrum at each pixel in a scan—has proven to be of significant use in mapping and correlating variations in the spectral emission parameters of epilayers,^{2,3} multi-quantum well (MQW) heterostructures,⁴ and optoelectronic nanostructures.^{5–7} However, luminescence is just one of the many consequences of the interaction of the electron beam with the material. If the device under excitation is connected to a closed circuit, a portion of the generated charge carriers can escape the material and be measured as the electron beam induced current (EBIC), provided there is a driving force in the circuit. In LEDs, the built-in field at the p - n junction acts as a driving force to separate excess carriers generated in the depletion region. EBIC can act as a complementary technique to CL because it adds further information about the behavior of generated charge carriers.^{3,8,9} They will undergo one of three mutually exclusive processes: radiative recombination, nonradiative recombination or escape to the circuit. This is represented by the following equation:

$$G = R_{\text{NR}} + R_{\text{R}} + I_{\text{EBIC}}/q, \quad (1)$$

where G is the generation rate, R_{NR} and R_{R} the non radiative and radiative recombination rates, respectively and I_{EBIC} the EBIC current. Since CL gives a measure of R_{R} and EBIC directly measures I_{EBIC} , an indirect measure of relative non-radiative recombination is made possible by simultaneous measurement of CL and EBIC.

Carrier recombination and transport in LEDs are also strongly influenced by the applied electric field, both across the whole depletion region in the form of carrier overshoot and capture^{10–13} and also in the quantum wells themselves via tunneling^{13,14} and the quantum-confined Stark effect (QCSE).¹⁵ Consequently, the applied voltage greatly affects the intensity and spectral characteristics of the CL spectrum as well as the EBIC. Both drift (Eq. (2)), whereby excess electrons and holes are swept out of the depletion region by the net field, and tunneling (Eq. (3)) through the quantum barriers, act to remove carriers from the active region:

$$\mathbf{J}_{\text{drift}} \propto \mathbf{F}, \quad (2)$$

$$\mathbf{J}_{\text{tunnel}} \propto \exp(-\Delta E/F), \quad (3)$$

where $\mathbf{J}_{\text{tunnel}}$ and $\mathbf{J}_{\text{drift}}$ are the components of the current density due to tunneling and drift, respectively, ΔE is the barrier height and \mathbf{F} the electric field.

Above the LED turn-on voltage forward diffusion current dominates and electroluminescence (EL) occurs due to recombination of the injected carriers. Thus to avoid overlap of CL and EL signals all electron beam measurements were made below the turn-on voltage when the EL intensity is low. When a reverse bias is applied, the junction field strength and the width of the depletion region both increase. This has the effect of increasing the induced current at the expense of the rates of both forms of recombination. Under

forward bias, the field is compensated, reducing carrier loss mechanisms and leading to an increase in recombination in the active region.

The field also affects the spectral characteristics of the luminescence via the QCSE. In InGaN/GaN quantum wells grown along the polar c -axis, the difference in the piezoelectric constants of GaN and InGaN results in band bending in the quantum barriers and wells due to the sheet charge build up at each well/barrier interface. In our devices, this induced piezoelectric field is in the opposite direction to the built-in field of the p - n junction. As such, forward biasing the diode increases the magnitude of the band bending in the quantum wells, increasing the redshift, while a reverse bias acts to flatten the band and blueshift the near-band-edge emission.

In this paper, we have used a combined CL/EBIC technique, with applied bias, to spatially map the variations of, and correlation between, the optical and electronic properties of an InGaN/GaN LED.

II. METHOD

The LED samples were grown by metal organic chemical vapor deposition (MOCVD) on (0001) sapphire, with a $2\text{ }\mu\text{m}$ n -type GaN layer doped to $5 \times 10^{18}\text{ cm}^{-3}$, a 5-period InGaN/GaN MQW active region emitting at around 490 nm and a 140 nm p -GaN cap with a measured carrier concentration of $3 \times 10^{17}\text{ cm}^{-3}$. The quantum wells and GaN barriers were $2.4 \pm 0.1\text{ nm}$ and $6.9 \pm 0.1\text{ nm}$, respectively. The grown wafers were processed into $1 \times 1\text{ mm}^2$ mesa etched, side contacted LEDs with an $\sim 10\text{ nm}$ thick oxidized Ni/Au semi-transparent current spreading Ohmic contact on the p -layer. Non-alloyed Ti/Al contact stripes were formed on the n -layer (as an Ohmic contact) and over the Ni/Au in an interdigitated arrangement that minimizes current crowding.

We performed electron beam measurements at room temperature using the scanning stage of modified electron probe microanalyser (EPMA). Due to the thickness of the p -type GaN layer on top of the active region, we used a beam voltage of 10 kV so that the maximum of the carrier generation profile lay close to the depletion region of the LED. Since the luminescence of interest is from the quantum wells, this is the optimal acceleration voltage; using a lower or higher voltage/penetration depth would mean that quantum well luminescence observed would come from generated charge carriers which had to diffuse through the p -GaN or n -GaN (respectively) to the active region. To reduce any damage to the sample, which would have affected subsequent measurements of a given area, we used a low beam current of 1 nA and defocused the spot to a diameter of $1\text{ }\mu\text{m}$.

A DC source/measure unit (Keithley 2401) was used to drive the devices and also to record the beam induced current. The applied bias was varied from -2 V to $+1.5\text{ V}$ in 0.5 V steps. The stage was scanned and at each point in the stage scan a full CL spectrum was collected by a CCD camera to build up a hyperspectral data-set. The CCD was set to trigger the source/measure unit to take readings of the beam induced current at each spectral acquisition, building up a beam induced current image simultaneously with the CL hyperspectral image. We analyzed the hyperspectral data

sets using our own software and fitted each spectrum with a Voigt peak to extract 2D maps of peak intensity, position, and width. The induced current maps were corrected for the diode “dark” current at each voltage by subtracting from every pixel a fixed value of the current, measured while the beam was switched off. Unless otherwise stated, all EBIC results presented are based on these corrected currents, i.e., only the extra current which the electron beam itself induces. Maps of the EBIC were plotted and analysed using the same software to compare the luminescence spectra to the induced current across the scanned area. Electroluminescence (EL) mapping was also performed by using a $8\text{ }\mu\text{m}$ pinhole as the entrance aperture of the spectrometer, producing maps with a spatial resolution of around $3\text{ }\mu\text{m}$.

III. RESULTS

Figure 1 shows typical spectra (b) and maps of fitted CL intensity (a), and EBIC (c) of a $49 \times 44\text{ }\mu\text{m}^2$ region of the LED from a device at short circuit (0 V). The dominant features in each map are patches around $5\text{--}10\text{ }\mu\text{m}$ in size which appear dark in both the CL and EBIC and also blue shifted. Given the independent nature of the three processes described in Eq. (1) these areas must have a higher rate of nonradiative recombination. The background signal in both these maps appears uniform, but this is not unexpected since InGaN (Ref. 16) material unlike binary GaN (Ref. 17) is found to be generally non uniform in EBIC and CL. Fig 1(d) plots the average MQW CL intensity and induced current for each map (averaged over all the pixels in the map) as a function of bias and shows their reciprocal nature, whereby the increase in electric field draws carriers away from the active region. The changes in CL and EBIC are not linear and increase significantly at around -0.5 V , due to the flattening of the band structure around the p - n junction beyond this point.

A comparison of the electron beam measurements with the EL was made in order to investigate if the variations seen in the CL affect the luminescence uniformity of the device when under operation. Mapping of coincident CL, EBIC, and EL is shown in Figure 2. The area mapped is a different one to that from Fig. 1 but is from the same die. The dark spots are apparent in all three of the CL, EBIC, and EL maps although with lower resolution in the EL due to the limiting size of the collection pinhole. However, additional features are visible in both the EL and EBIC. Large filament type structures with bright contrast run across the mapped area in the EBIC and EL data. These areas also correlate with a significant blueshift, of around 30 meV , in the EL emission peak. The EL was measured at 100 mA (the CL/EBIC was collected, as before, at 0 V) where the dominant effect upon the emission wavelength is likely to be screening of the QCSE by the high free carrier density (heating effects were reduced by using a pulsed current source with 4% duty cycle). However, no such contrast exists in the CL. A lower nonradiative recombination rate would be consistent with the increased EL and EBIC, but increased brightness in the CL would be expected if that were the cause. Only variations in and around quantum wells will contribute to the CL, and so

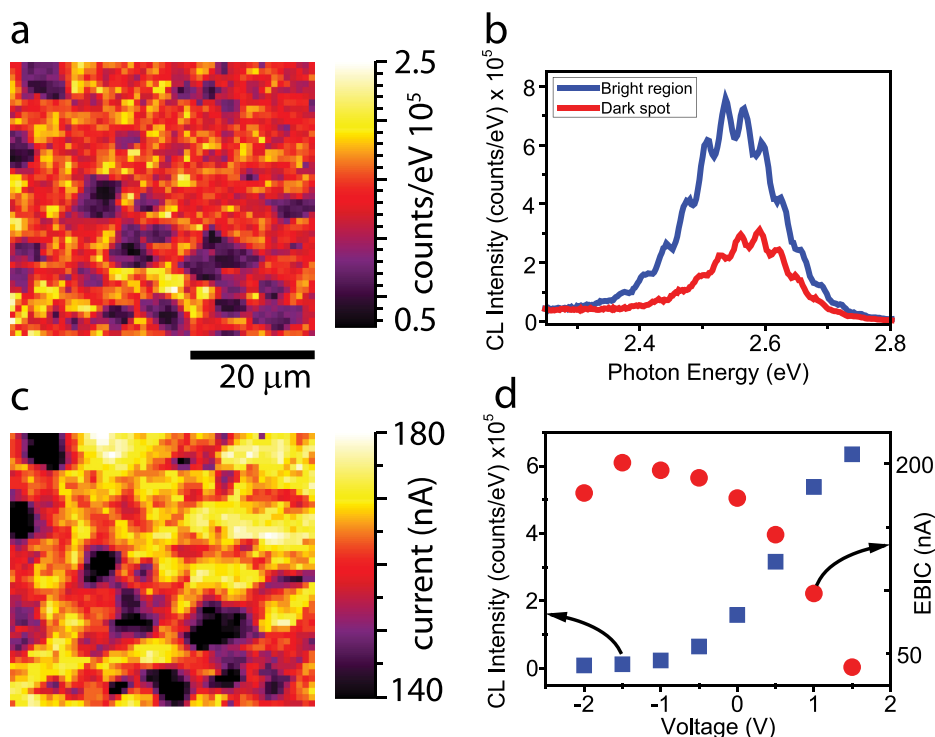


FIG. 1. Maps acquired of the LED at 0 V of (a) the fitted CL peak intensity, (b) the fitted CL peak center and (c) the electron beam induced current (d) CL intensity (squares) and EBIC (circles) vs. applied bias.

the bright filament areas in the EL and EBIC could come from patches of increased conductivity in the *p*-type and/or *n*-type layer which do not directly affect CL intensity. Such areas would have higher carrier densities and would therefore be brighter in EL, allow a larger EBIC to escape from the depletion region. This would also explain the approximate 30–40 meV blue shift which is observed in these areas.

Higher free carrier density would act to screen the built-in piezoelectric fields, counteract the band bending in the quantum wells and so reduce the QCSE which would blueshift the emission peak.

The change in CL and EBIC as a function of bias is shown in Figure 3 where maps collected with the device under biases of +1.5 V, 0 V, and −2 V are shown. As shown

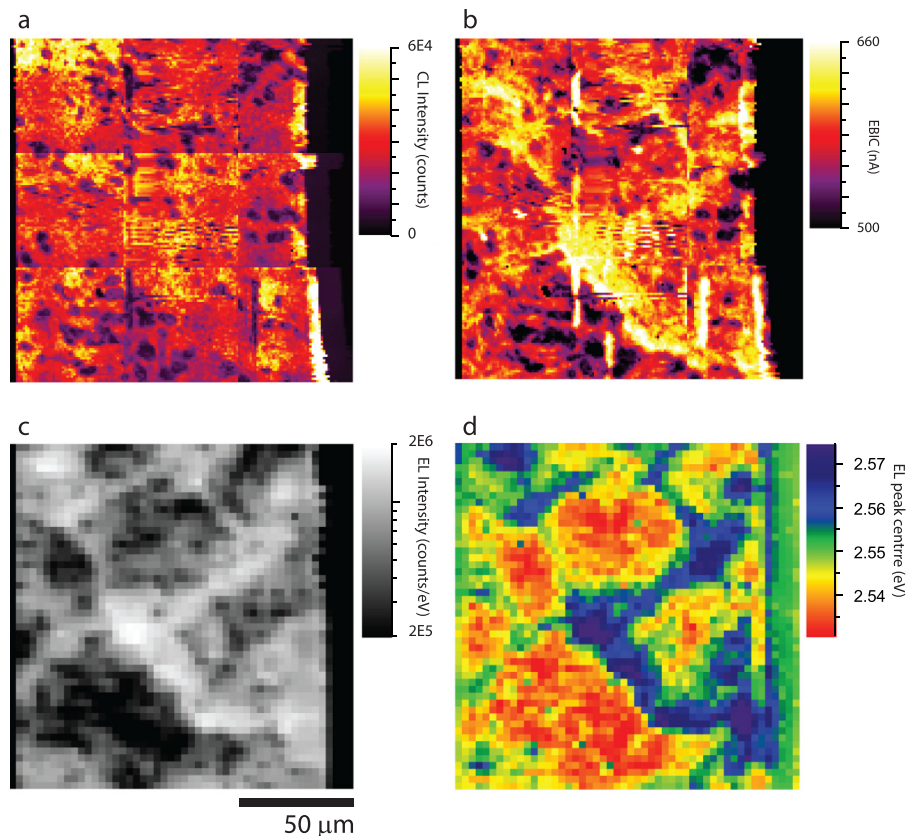


FIG. 2. Maps, from a different area showing the correlation between CL (a), EBIC (b) (both at 0 V), and EL intensity (c) and peak position (d) at 100 mA, 3.2 V.

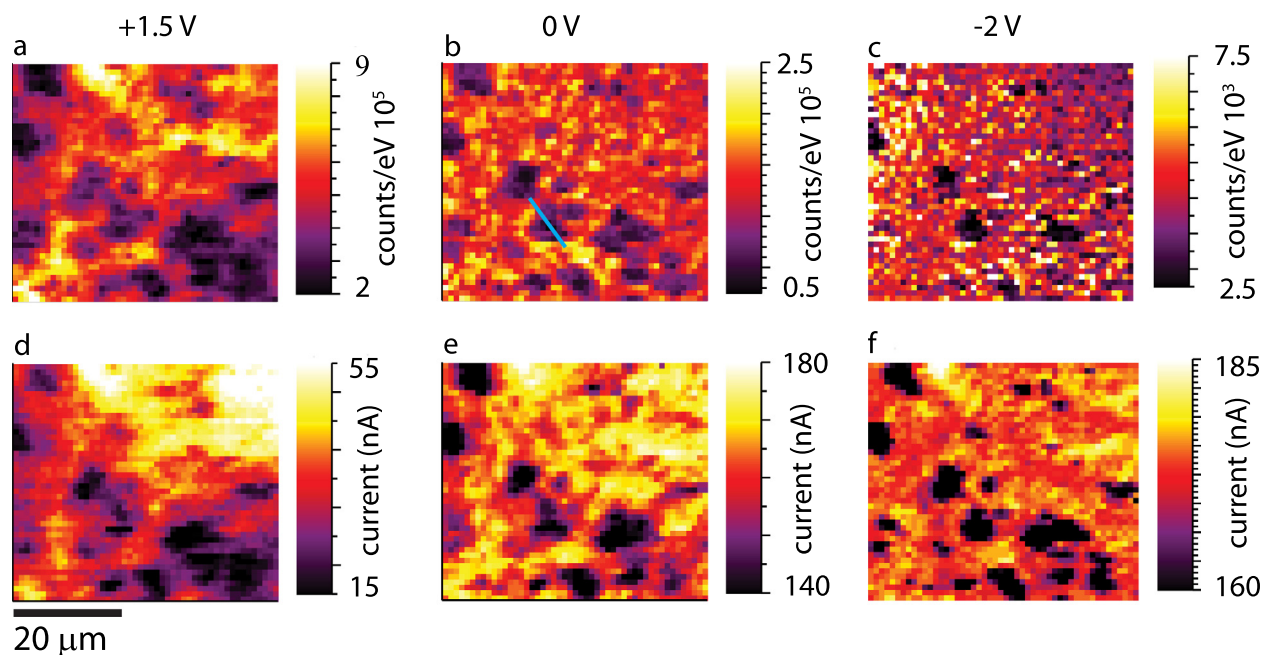


FIG. 3. Maps of the cathodoluminescence intensity (a)–(c) and EBIC (d)–(f) at +1.5, 0, and -2 V. The blue line in (b) shows the line scan which is presented in Figure 4(a).

in Fig. 1(d), a drop in voltage from $+1.5$ V to -2 V causes the CL intensity to decrease and the induced current to increase, which fits the model of a larger electric field driving carriers out of the active region. It is evident from the CL maps that as the electric field in the junction is increased (i.e., a more negative applied bias) both the size and number of the dark features appears to decrease. To quantify the change, linescans were extracted from across several dark spots on the CL intensity and EBIC maps at each bias. The scans from $+1.5$ V and -2 V in the CL are shown in Fig. 4(a). The traces show that the width of the dark areas is markedly reduced as the reverse bias increases. The size of the spots was estimated by measuring the FWHM of the central dips in the linescan and the results for all 8 maps in the bias series are shown in Fig. 4(b). In the CL case, there is a linear increase in feature size from about $3\text{ }\mu\text{m}$ to $7\text{ }\mu\text{m}$ as the junction field is decreased. The EBIC data show no clear change in spot size with bias. The error bars in the plots are due to the variation in the sizes of the dark spots across the sample. In the CL data, the error bar seem to decrease closer to 0 V though it is not obvious why this would be the case. The spot size increase is within the plane of the quantum well, while the processes of carrier capture and escape are primarily in the growth direction, perpendicular to the plane of the wells. When the band structure in the c -direction (outside the quantum wells) is flatter (i.e., at forward bias), these processes are slower due to reduced drift velocity, giving the carriers longer to diffuse within the QW plane before recombining, thus explaining the increased feature sizes in CL. The invariance of the EBIC size is likely due to the fact that the EBIC current consists mostly of charge carriers which have drifted out of the active region, as opposed to tunneling.⁹ The carriers have a kinetic energy too large to be captured by the quantum wells and therefore are not sensitive to diffusion in the quantum well plane. Since the CL comes

only from the quantum wells themselves we infer that EBIC contrast on this scale is affected by variation somewhere in the active region. However, since the majority of our EBIC

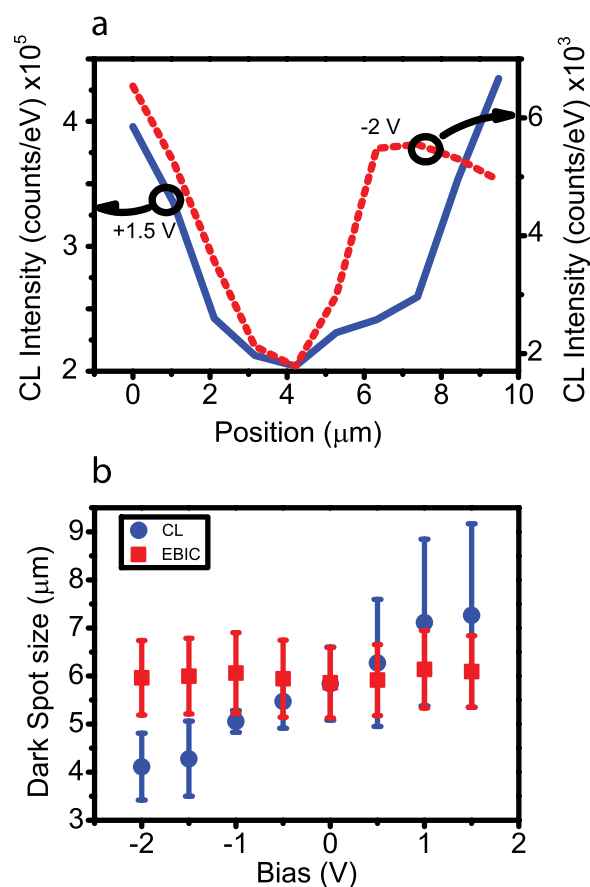


FIG. 4. (a) CL linescans taken from across the single dark spot indicated on map, at $+1.5$ V (solid line) and -2 V (dashed line), and (b) estimated size of dark feature in CL (circles) and EBIC (squares) vs. bias.

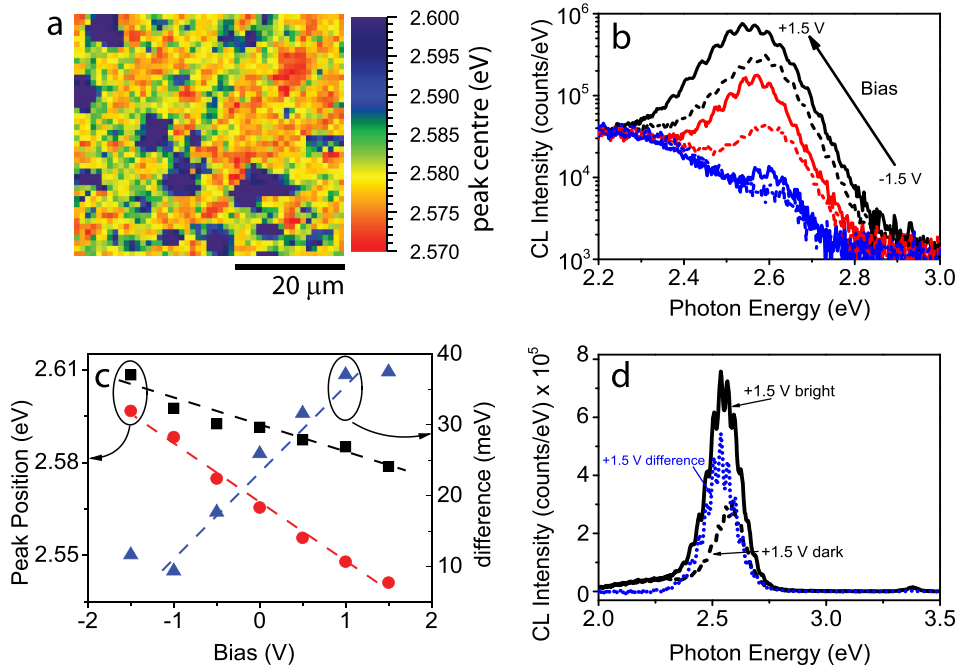


FIG. 5. (a) Map of the fitted cathodoluminescence spectral peak energy at 0 V; (b) Sample spectra, centered on the MQW emission band, from bright area (solid lines) and dark spot (dashed lines) at -1.5 , 0 and $+1.5$ V; (c) peak position as a function of bias for bright area (circles), dark spots (squares) and the difference (triangles) (the dashed lines are guides to the eye); and (d) subtraction of dark area spectrum from bright area spectrum at $+1.5$ V highest peak in the from a bright area, lowest from a dark area and the dotted line is the difference.

current is due to carriers not captured by the quantum wells,⁹ we must conclude that whatever defect causes the decrease in CL intensity inside the quantum wells, must also affect the entire depletion region. This implies that variation in the EBIC is observed on two levels: firstly in the large scale filament structures which, due to correlation with higher EL intensity and emission energy and lack of correlation with CL, are likely due to variations in conductivity in the p/n type layers. Second, a spottiness in the optically active region which correlates with the dark spots in CL.

The CL from spectra the dark spots are also found to be blueshifted, with respect to the background, by between 10 and 40 meV depending on applied bias. At 0 V the blue shift is approximately 20 meV, as seen in Figure 5(a). Fig. 5(b) shows example spectra taken from a dark spot and a bright area at $+1.5$ V, 0 V, and -1.5 V. Only the peak associated with the quantum well is shown. The rising background on the low energy side could be attributed to parasitic cyan emission¹ or the yellow defect band, excited in the *n*-GaN by the electron beam. In each of the series of spectra, there is an approximately two orders of magnitude drop in intensity, accompanied by a blue shift. Fig. 5(c) plots the peak position, as a function of bias, for an average of several dark spots and bright areas and the difference between these two values. The graph shows that, while the emission from the dark and bright areas both red shift with increasing bias, the peaks in the dark spot spectra only shift by around 30 meV with those from the brighter areas changing by almost twice as much. The voltage drop across the active region acts to change the potential inside the quantum wells. Assuming an abrupt *p-i-n* junction, the field in the depletion region can be expressed as¹⁸

$$E_{dp} = \frac{2\sqrt{V_{bi}(V_{bi} - V_a)}}{W_0}, \quad (4)$$

where E_{dp} is the electric field across the depletion region, V_{bi} is the built-in voltage, V_a is the applied bias, and W_0 is the

width of the depletion region in thermal equilibrium. Using the values of N_d and N_a quoted in the introduction along with literature values of the intrinsic carrier concentration of GaN, V_{bi} and W_0 were calculated, respectively, to be 3.3 V and ~ 100 nm. Since our concern is the effect of the *change* in bias upon the *change* in transition energy it was sufficient to calculate the electric field, using eqn 4, at the two extremes of our applied biases (± 1.5 V). The change in electric field was found to be 3.085×10^5 V/cm. Across each quantum well of 2.4 nm, the resultant change in potential energy of the charge carriers is 3.12×10^5 V/cm \times 2.4 nm = 74 mV, or 74 meV per charge carrier.

The experimentally observed shift, in the bright regions, of ~ 61 meV, is within 15% of the calculated effect of the change in bias. The difference could be due to a number of factors. Firstly, the change in carrier energy is not trivially linked to the potential energy change in the well due to the offset added to the band structure by the QCSE. Secondly, based on previous arguments, the number of electron/hole pairs in and around the depletion region is not invariant with applied bias; at larger reverse biases more charge contributes to the EBIC. As a consequence, the screening of the QCSE also diminishes and this would reduce the observed blue-shift as the reverse bias increases: in effect adding a linear offset to the peak position plot. Given these additional effects, it is likely that the biggest contribution to the peak shift in the bright areas is the change in electric field caused by the applied bias. In the dark regions however, the shift is much smaller and this implies that something more complicated is going on here; in order for the 30 meV shift seen in these areas to be accounted for purely by the change in applied electric field would require either a lower electric field across the depletion region or a reduction in the thickness of the quantum wells. A more probable cause is related to the correlation of the peak position with the lower EBIC and CL intensity. An explanation for the dark spots based purely on areas of increased nonradiative recombination

cannot account for the large blue shift. The drop in EBIC could be due to increased trapping of carriers in these area by defects. This extra charge would act to blue shift the spectra through screening of the QCSE. This explains both the difference in peak positions between the dark spots and bright areas and why the change in peak position occurs at a different rate, as a function of bias, in the two areas.

The presence of dark CL/EBIC spots on a 2–10 μm scale is intriguing and possible causes are now considered. Leading candidates would be the effects of decomposition of the InGa_N within the quantum wells or the impact of threading dislocations (TDs). Local variations in the In_N content, or in the well thicknesses (which have the same effect¹⁹), occur on a nanometer scale. These average out on a micron scale and would not cause the features observed in the EBIC/CL. Electron channeling contrast imaging (ECCI)²⁰ has been used to estimate the TD density, which is found to be around $5 \times 10^8 \text{ cm}^{-2}$. Based on this density, the number of TDs in our 2500 μm^2 area would be over 10 000 and we can conclude that the observed dark spots are not due to individual dislocations. Clustering of dislocations is possible but no evidence for TD clustering on the relevant scale can be seen in atomic force microscopy (AFM) images from devices where the growth has been terminated after the active region. The observed blueshift of the dark spots relative to the background, together with the change in the shift of the CL peaks with applied bias, indicate that they are associated with a trapping of charge on the micron scale in the active region. The charge traps increase non-radiative recombination in the QWs within the dark spots and a likely candidate is a clustering of point defects within the active region.

IV. CONCLUSION

In conclusion, we have used a combination of cathodoluminescence and beam induced current under applied bias to simultaneously investigate the luminescence and conductivity variations across an InGa_N/Ga_N LED as a function of the electric field across the active region. Large domains ($\sim 100 \mu\text{m}$) of increased conductivity in either the *p*-type or *n*-type material were revealed by a correlation of bright contrast in EL and EBIC, with an absence of correlation in CL indicating that the effect does not originate in the quantum wells. Small regions in the quantum wells, around 2–10 μm across, were found to yield lower signals for both cathodoluminescence and beam induced current, indicating areas of increased nonradiative recombination. The observed sizes of the dark spots in the CL maps change with applied bias, becoming larger as the field across the depletion region is

reduced and the free carriers are able to diffuse further in the plane of the quantum well before recombining. The spectral emission was blue shifted within the dark regions, possibly due to an increase in carrier trapping in the depletion region and subsequent increased screening of the QCSE.

ACKNOWLEDGMENTS

Funding for lead author from EPSRC grant no. EP/I012591/1 “Lighting the Future”. Thanks go to Institute of Photonics (Strathclyde) for use of wire bonder and Dr. Jochen Bruckbauer for helpful discussions.

- ¹A. Mao, Q. Cho, E. Dai, E. F. Schubert, J. K. Son, and Y. Park, *Appl. Phys. Lett.* **98**, 023503 (2011).
- ²J. Christen, M. Grundmann, and D. Bimberg, *J. Vacuum Sci. Technol. B: Microelectron. Nanometer Struct.* **9**, 2358 (1991).
- ³M. Avella, E. de la Puente, J. Jimenez, A. Castaldini, A. Cavallini, and L. Polenta, *J. Cryst. Growth* **210**, 220 (2000).
- ⁴J. Bruckbauer, P. R. Edwards, T. Wang, and R. W. Martin, *Appl. Phys. Lett.* **98**, 141908 (2011).
- ⁵P. R. Edwards, D. Sleith, A. W. Wark, and R. W. Martin, *J. Phys. Chem. C* **115**, 14031 (2011).
- ⁶K. J. Lethy, P. R. Edwards, C. Lui, W. N. Wang, and R. W. Martin, *J. Appl. Phys.* **112**, 023507 (2012).
- ⁷T. Zhu, A. El-Ella, B. Reid, M. J. Holmes, R. A. Taylor, M. J. Kappers, and R. A. Oliver, *J. Cryst. Growth* **338**, 262 (2012).
- ⁸A. Boudjani, B. Sieber, F. Cleton, and A. Rudra, *Mater. Sci. Eng. B* **42**, 192 (1996).
- ⁹U. Jahn, S. Dhar, M. Ramsteiner, and K. Fujiwara, *Phys. Rev. B* **69**, 115323 (2004).
- ¹⁰X. N. U. O. Xing Li, H. Lui, and H. Morkoc, *Superlattices Microstruct.* **47**, 118 (2010).
- ¹¹J. P. Liu, J. H. Ryou, R. D. Dupuis, J. Han, G. D. Shen, and H. B. Wand, *Appl. Phys. Lett.* **93**, 021102 (2008).
- ¹²O. Ozgur, X. Ni, X. Li, J. Lee, S. Liu, S. Okur, V. Avrutin, A. Matulionis, and H. Morkoc, *Semicond. Sci. Technol.* **26**, 014022 (2011).
- ¹³H. A. K. F. A. Satake and K. Soejima, *Phys. Status Solidi C* **3**, 2203 (2006).
- ¹⁴Y. D. Jho, J. S. Yahng, E. Oh, and D. S. Kim, *Appl. Phys. Lett.* **79**, 1130 (2001).
- ¹⁵H. Masui, J. Sonoda, N. Pfaff, I. Koslow, S. Nakamura, and S. P. DenBaars, *J. Phys. D: Appl. Phys.* **41**, 165105 (2008).
- ¹⁶A. Cremades and J. Piqueras, *Mater. Sci. Eng. B* **91–92**, 341–344 (2002).
- ¹⁷E. B. Yakimov, P. S. Vergeles, A. V. Govorkov, A. Y. Polyakov, N. B. Smirnov, In.-H. Lee, C. R. Lee Cheul, and S. J. Pearton, *Superlattices Microstruct.* **45**, 308–313 (2009).
- ¹⁸D. Neamen, *Semiconductor Physics and Devices: Basic Principles*, 4th ed. (McGraw-Hill Higher Education, New York, 2012), Chap. 7.
- ¹⁹R. A. Oliver, F. C.-P. Massabuau, M. J. Kappers, W. A. Phillips, E. J. Thrush, C. C. Tartan, W. E. Blenkhorn, T. J. Badcock, P. Dawson, M. A. Hopkins, D. W. E. Allsopp, and C. J. Humphreys, *Appl. Phys. Lett.* **103**, 141114 (2013).
- ²⁰N.-K. Gunasekar, J. Bruckbauer, P. R. Edwards, S. Krausel, B. Hourahine, R. W. Martin, M. J. Kappers, M. A. Moram, S. Lovelock, R. A. Oliver, C. J. Humphreys, and C. Trager-Cowan, *Microsc. Microanal.* **20**, 55–60 (2014).